

# Deepest Sensitivity to Wavelike Dark Photon Dark Matter with SRF Cavities

R. Cervantes,<sup>1,\*</sup> C. Braggio,<sup>2,3</sup> B. Giaccone,<sup>1</sup> D. Frolov,<sup>1</sup> A. Grasselino,<sup>1</sup>  
R. Harnik,<sup>1</sup> O. Melnychuk,<sup>1</sup> R. Pilipenko,<sup>1</sup> S. Posen,<sup>1</sup> and A. Romanenko<sup>1</sup>

<sup>1</sup>*Fermi National Accelerator Laboratory, Batavia IL 60510*

<sup>2</sup>*Dip. di Fisica e Astronomia, Università di Padova, 35100 Padova, Italy*

<sup>3</sup>*INFN - Sezione di Padova, 35100 Padova, Italy*

(Dated: August 8, 2022)

Wavelike, bosonic dark matter candidates like axion and dark photons can be detected using microwave cavities commonly referred to as haloscopes. Traditionally, haloscopes consist of tunable copper cavities operating in the  $TM_{010}$  mode, but the performance of these cavities has been limited by ohmic losses. In contrast, superconducting radio frequency (SRF) cavities can achieve quality factors of  $\sim 10^{10}$ , perhaps five orders of magnitude better than copper cavities, which would lead to more sensitive dark matter detectors. In this paper, we first derive that the scan rate of a haloscope experiment is proportional to the loaded quality factor  $Q_L$ , even if the cavity bandwidth is much narrower than the dark matter halo lineshape. We then present a proof-of-concept search for dark photon dark matter using a non-tunable ultra-high quality SRF cavity. We exclude dark photon dark matter with kinetic mixing strengths of  $\chi > 2 \times 10^{-16}$  for a dark photon mass of  $m_{A'} = 5.37 \mu\text{eV}$ , achieving the deepest exclusion to wavelike dark photons by almost an order of magnitude.

## I. INTRODUCTION

There is overwhelming evidence that 84.4% of the matter in the universe is made out of dark matter (DM) [1–7]. The  $\Lambda\text{CDM}$  model describes dark matter as feebly interacting, non-relativistic, and stable on cosmological timescales. Not much else is known about the nature of dark matter, particularly what particles beyond the standard model it is made of.

The dark photon (DP) is a compelling dark matter candidate. It is a spin-1 gauge boson associated with a new Abelian  $U(1)$  symmetry. It is one of the simplest possible extensions to the Standard Model (SM) [8–10]. The dark photon, having the same quantum numbers as the SM photon, generically interacts with the SM photon through kinetic mixing [11, 12] described by the Lagrangian

$$\mathcal{L} = -\frac{1}{4}(F_1^{\mu\nu}F_{1\mu\nu} + F_2^{\mu\nu}F_{2\mu\nu} - 2\chi F_1^{\mu\nu}F_{2\mu\nu} - 2m_{A'}^2 A'^2), \quad (1)$$

where  $F_1^{\mu\nu}$  is the electromagnetic field tensor,  $F_2^{\mu\nu}$  is the dark photon field tensor,  $\chi$  is the kinetic mixing strength,  $m_{A'}$  is the DP mass, and  $A'$  is the DP gauge field. If both  $m_{A'}$  and  $\chi$  are sufficiently small, then it is stable on cosmological timescales, with three photons or neutrinos being the only available decay channels [13]. The dark photon is then an attractive dark matter candidate. If its mass is less than an eV, the DPDM is in the wavelike regime, where it is best described as a coherent wave oscillating at the frequency of its rest mass rather than a collection of particles. The dark matter kinetic energy distribution sets the degree of coherence of wavelike dark matter to be of order  $v_{\text{DM}}^2 \sim 10^{-6}$  [14, 15].

Several mechanisms could produce a relic of cosmic dark photons. One simple example is the displacement of the DP field through quantum fluctuations during inflation [16]. These fluctuations in the DP field serve as the initial displacement for dark photon field oscillations which commence once the Universe’s expansion rate falls below the DP mass. Other mechanisms are possible and are described in [10, 17].

Dark photon dark matter (DPDM) can be detected through their mixing with the SM photon. If dark photons oscillate into SM photons inside a microwave cavity with a large quality factor, then a feeble EM signal accumulates inside the cavity, which can be read by ultra-low noise electronics. This type of detector is called a haloscope and is often deployed to search for axionic DM [18]. The SM photon frequency  $f$  is related to the dark photon energy  $E_{A'}$  by the relationship  $f = E_{A'}$  (using natural units).

The dark photon signal power is [9, 19–21], in natural units,

$$P_S = P_0 \frac{\beta}{\beta + 1} L(f, f_0, Q_L) \quad (2)$$

$$P_0 = \begin{cases} \eta \chi^2 m_{A'} \rho_{A'} V_{\text{eff}} Q_L, & \text{if } Q_L \ll Q_{DM} \\ \eta \chi^2 m_{A'} \rho_{A'} V_{\text{eff}} Q_{DM}, & \text{if } Q_L \gg Q_{DM} \end{cases} \quad (3)$$

$$V_{\text{eff}} = \frac{(\int dV \mathbf{E}(\vec{x}) \cdot \mathbf{A}'(\vec{x}))^2}{\int dV \epsilon_r |\mathbf{E}(\vec{x})|^2 |\mathbf{A}'(\vec{x})|^2} \quad (4)$$

where  $\eta$  is a signal attenuation factor,  $\rho_{A'}$  is the local density of dark matter,  $V_{\text{eff}}$  is the effective volume of the cavity,  $Q_L$  is the cavity’s loaded quality factor,  $Q_{DM}$  is the dark matter “quality factor” related to the dark matter coherence time, and  $\beta$  is the cavity coupling coefficient. The Lorentzian term is  $L(f, f_0, Q_L) = 1/(1+4\Delta^2)$ , where  $\Delta \equiv Q_L(f - f_0)/f_0$  is a detuning factor that depends on the SM photon frequency  $f$ , cavity resonant

\* Correspondence to: raphaelc@fnal.gov

frequency  $f_0$ , and  $Q_L$ .  $V_{eff}$  is the overlap between the dark photon field  $\mathbf{A}'(\vec{x})$  and the dark photon-induced electric field  $\mathbf{E}(\vec{x})$ . Equations 2, 3, and 4 assume that the cavity size is much smaller than the DP de Broglie wavelength.

The dark photon mass is unknown, so haloscopes must be tunable to search through the  $\chi$  vs.  $m_{A'}$  parameter space. The scan rate for haloscope experiments is a key figure of merit strongly dependent on the SNR. The SNR for a haloscope signal is  $\text{SNR} = (P_S/P_n)\sqrt{b\Delta t}$  [22, 23], where  $P_n$  is the noise power,  $b$  is the frequency bin width and  $\Delta t$  is the integration time.  $P_n$  is the combination of the cavity's blackbody radiation and the receiver's Johnson noise. The noise power can be expressed as  $P_n = Gk_b b T_n$ , where  $k_b$  is the Boltzmann constant,  $G$  is the system gain, and  $T_n$  is the system noise temperature referenced to the cavity.

If  $Q_L \gg Q_{DM}$ , the cavity width is smaller than the dark matter halo lineshape width  $\Delta f_{DM}$ . The resulting dark matter signal will follow the Lorentzian cavity response with bandwidth  $\Delta f_c = f_0/Q_L$ . Fortunately, a haloscope is sensitive to a distribution of possible dark photon rest masses corresponding to the cavity resonant frequency  $f_c$ . In other words, a single cavity tuning step can probe the entire dark matter lineshape bandwidth, and the tuning steps need only to be comparable to  $\Delta f_{DM}$ .

The frequency bin width  $b$  is typically chosen to be comparable to the dark matter signal bandwidth. Typical haloscope experiments use copper cavities with  $Q_L \ll Q_{DM}$ , so  $b \sim \Delta f_{DM} = f_0/Q_{DM}$ . However, if  $Q_L \gg Q_{DM}$ , the signal bandwidth is the same as the cavity bandwidth and  $b \sim f_0/Q_L$ . This means that the noise power is inversely proportional the  $Q_L$ , i.e.,  $P_n \sim Gk_b (f_0/Q_L) T_n$ . The higher  $Q_L$  is, the lower the noise power.

An estimate of the integration time can be obtained by rearranging the SNR equation  $\Delta t = 1/b (\text{SNR} \times P_n/P_S)^2$ .

The tuning steps are  $\Delta f \sim f_0/Q_{DM}$ . Putting all this together, the scan rate for a dark photon haloscope consisting of an ultra-high Q microwave cavity, i.e.,  $Q_L \gg Q_{DM}$  is

$$\frac{df}{dt} = \frac{\Delta f}{\Delta t} \sim Q_L Q_{DM} \left( \frac{\eta \chi^2 m_{A'} \rho_{A'} V_{eff} \beta}{\text{SNR} T_n (\beta + 1)} \right)^2. \quad (5)$$

The scan rate equation, Equation 5, happens to be the same whether  $Q_L \gg Q_{DM}$  or  $Q_L \ll Q_{DM}$  [24]. In both cases, the scan rate is directly proportional to  $Q_L$ . It behooves the community to achieve the highest  $Q_L$  possible as it is perhaps the only parameter in Equation 5 that can increase by many orders of magnitude<sup>1</sup>.

<sup>1</sup>  $V_{eff}$  may also increase substantially using multi-wavelength haloscope designs [24–31].

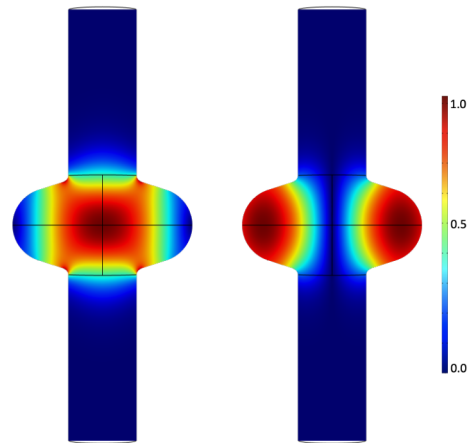


FIG. 1. Normalized electric (left) and magnetic (right) field intensity of the TM010 mode in a cross section through the middle of a TESLA cavity used in particle accelerators. Figure is from [35].

As a comparison, ADMX uses copper cavities with  $Q_L \sim 8 \times 10^4$  [32], whereas niobium SRF cavities can achieve  $Q_L \sim 10^9 - 10^{11}$  depending on the temperature and cavity treatment [33]. This suggests that SRF cavities can increase the instantaneous scan rate of haloscope experiments by as much as a factor of  $10^5$ .

## II. DARK PHOTON DARK MATTER SEARCH WITH AN SRF CAVITY

The Superconducting Quantum Materials and Systems (SQMS) Center, hosted by Fermilab, performs a wide range of multidisciplinary experiments with SRF cavities. An experiment studying the material properties of an SRF cavity for temperatures below 1 K was underway when it was decided that a dark photon dark matter search should be performed with the same cavity. This proof-of-principle search using a  $Q_L \approx 8 \times 10^9$ , a HEMT amplifier, and the standard haloscope analysis is enough to demonstrate superior sensitivity to wavelike dark photons compared to previous searches.

### A. Experimental Setup

The haloscope consists of a TESLA-shaped single-cell niobium cavity [34] with TM<sub>010</sub> resonant frequency  $f_0 \approx 1.3$  GHz. The cavity is made of fine-grain bulk niobium with a high residual resistivity ratio of  $\simeq 300$ . The associated electric and magnetic field distribution is shown in Fig. 1. The cavity volume is 3875 mL, and the effective volume calculated from Equation 4 is  $V_{eff} = 669$  mL, assuming a randomly polarized DP field. Electromagnetic coupling to the cavities is performed using axial pin couplers at both ends of the beam tubes.

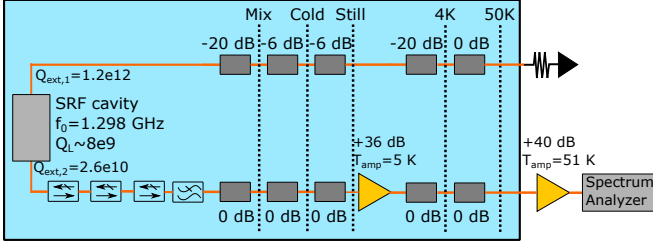


FIG. 2. The microwave electronics for the dark photon dark matter search. Power from the cavity is amplified by a cryogenic HEMT amplifier and a room temperature amplifier before reaching the spectrum analyzer. A series of isolators prevent the cavity from being excited by the amplifier’s noise.

The cavity underwent heat treatments in a custom-designed oven to remove the niobium pentoxide ( $\text{Nb}_2\text{O}_5$ ) and to mitigate the two-level system (TLS) dissipation [36, 37]. The central cell 1.3 GHz cavity is heat treated at  $\sim 450^\circ\text{C}$  in vacuum for eight hours.

The cavity is cooled to  $\approx 45\text{ mK}$  using a BlueFors XLD 1000 dilution refrigerator. A double-layer magnetic shielding around the entire cryostat is used, and magnetometers placed directly on the outside cavity surfaces indicate that the DC ambient magnetic field level is shielded to below  $2\text{ mG}$ .

A diagram of the microwave electronics is shown in Fig. 2. A series of attenuators on the cavity input line attenuates the room-temperature noise. The power from the cavity is first amplified by a cryogenic HEMT amplifier (LNF-LNC0.3.14A [38]). At  $1.3\text{ GHz}$ , the amplifier noise temperature is  $4.9(5)\text{ K}$  and the gain is about  $36\text{ dB}$ . The uncertainty in the amplifier noise temperature comes from private correspondence with Low Noise Factory, and additional references include [39, 40].

Between the HEMT and SRF cavity, there is a series of three microwave isolators (QuinStar QCY-G0110151AS circulators with the third port terminated) and a low pass filter (Mini-Circuits VLFX-1350+). The isolators prevent the HEMT amplifiers from injecting noise into the cavity. According to the manufacturer datasheets, the combined insertion loss is at maximum  $2.5\text{ dB}$ .

The signal is further amplified at room temperature using a Fairview FMAM1028 amplifier. The signal is then injected into the appropriate measurement device (spectrum analyzer, network analyzer, or phase noise analyzer).

## B. Characterization of Cavity and Microphonics

The cavity’s resonant frequency is identified using a self-excitation loop shown in Fig. 3. The thermal noise from the output of the cavity is amplified, phase-shifted, and fed back into the input of the cavity. The phase shifting is performed with an ATM P2506. A power splitter feeds the cavity’s output power to the spectrum analyzer

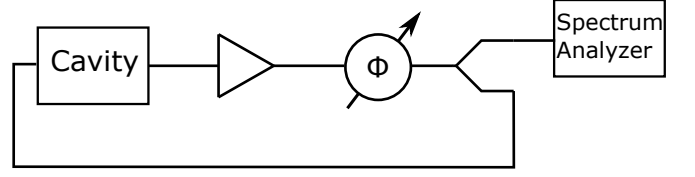


FIG. 3. A schematic for the self-excitation loop used to find the cavity’s resonant frequency and characterize microphonics.

to monitor the response to the self-excitation loop.

The resulting power is shown in Fig. 4. The central peak corresponds to the resonant frequency. There are sidebands spaced  $58\text{ Hz}$  apart from the central peak and a forest of smaller peaks. The power within the carrier peak and sidebands are confined within the cavity bandwidth. These sidebands are caused by the modulation of the resonant frequency due to microphonics, i.e., vibrations. These vibrations originate primarily from the dilution refrigerator’s pulse tubes. The sidebands are about  $13.5\text{ dB}$  smaller than the carrier frequency. A separate measurement with the Rohde & Schwarz FSWP Phase Noise Analyzer shows that for the modulation frequency  $58\text{ Hz}$ , the cavity peak frequency deviation from the resonant frequency is  $40(10)\text{ Hz}$ .

The microphonics were reduced substantially by turning off the pulse tubes. Fig. 4 show that the sidebands are  $31\text{ dB}$  smaller than the main carrier. Independent measurements with the phase noise analyzer show that for a modulation frequency  $58\text{ Hz}$ , the cavity peak frequency deviation is  $\approx 3.5\text{ Hz}$ . Since less than  $0.1\%$  of the power is spread to the sidebands, microphonics is a negligible effect when the pulse tubes are off. The pulse tubes were turned off for the dark photon dark matter search, and the cavity temperature was stable for over  $20\text{ min}$  before the pulse tubes were turned back on.

Turning off the pulse tubes to mitigate microphonics is not a viable strategy for an extended dark matter search scanning over a wide range of frequencies. It should be noted that these sidebands were not present in a previous operational run. This suggests that something in the mechanical structure loosened after the DR was thermally-cycled. Readjusting the mechanical structure and perhaps mechanically isolating the pulse tubes will likely mitigate the microphonics.

If microphonics cannot be mitigated, then the dark matter signal may be modeled as a frequency-modulated signal. This effect reduces the SNR of a dark matter signal because it spreads the dark matter signal over a larger bandwidth. But it is a quantifiable systematic that can be incorporated into the haloscope analysis.

The cavity’s loaded quality factor  $Q_L$  is measured using a decay measurement [41]. This decay measurement is implemented with a Keysight ENA Network Analyzer E5080B. At the resonant frequency, the network analyzer injects a  $15\text{ dBm}$  signal with a bandwidth of  $1\text{ kHz}$  into the input transmission line. Port 2 of the VNA measures

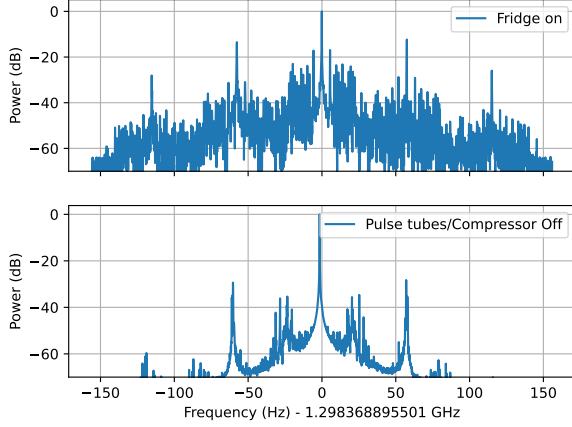


FIG. 4. Spectrum coming out of cavity from self-excitation loop. Microphonics, mostly from the dilution refrigerator pulse tubes, introduces a modulating effect. The sideband amplitude was greatly diminished by turning off the pulse tubes.

the absolute power from the cavity output line. The network analyzer source is then turned off, and the output power is observed to decay over several seconds until it reaches an equilibrium. The measured power is fitted using  $P_t = A \exp(-t/\tau_L)$ , and  $Q_L = 2\pi f_0 \tau_L$ . From these decay measurements, the loaded quality factor is conservatively determined to be  $Q_L = 8 \times 10^9$ .

The antenna external quality factors are measured beforehand in a separate test stand following the procedure outlined in Reference [42]. From the measured external quality factors  $Q_e$  and the measured  $Q_L$ , the cavity coupling coefficient of the cavity output port can be determined using  $\beta = (Q_L/Q_e) / (1 - Q_L/Q_e)$ . From the measured  $Q_L$  and  $Q_e$ ,  $\beta = 0.59 \pm 0.09$ .

### C. Dark Photon Dark Matter Search

For this proof-of-principle measurement, there is no tuning mechanism. A single power spectrum is measured. In the absence of a discovery, an exclusion on the kinetic mixing strength  $\chi$  is determined from the measured power spectrum, the system noise temperature, and cavity properties. The relevant properties for determining the dark photon signal power and system noise temperature are shown in Table I.

The signal attenuation factor  $\eta$  is determined from cascaded insertion loss of the three isolators and low-pass filter in between the cavity and cryogenic amplifier (Fig. 2). From the manufacturer datasheets, the maximum combined loss is 2.5 dB. The application of the Savitsky-Golay filter that is typical of haloscope analyses [43, 44] also attenuates a potential dark matter signal by 9%. This was determined by simulating an SNR=5 signal on resonance. The combination of these contributions leads

parameter	value
$\eta$	0.51
$\beta$	$0.59 \pm 0.09$
$V_{eff}$	669 mL
$\rho_{A'}$	$0.45 \text{ GeV/cm}^3$
$m_{A'}$	$5.3 \times 10^{-15} \text{ GeV}$
$\Delta t$	$1.5 \times 10^{27} \text{ GeV}^{-1}$ (1000 s)
$Q_L$	$8 \times 10^9$
$T_n$	$5.0(5) \times 10^{-13} \text{ GeV}$ (4.3(6) K)
$b$	$6.7 \times 10^{-25} \text{ GeV}$ (0.1625 Hz)

TABLE I. Operating parameters for the dark photon dark matter search with the SQMS SRF cavity. Values are displayed in natural units when appropriate so that they can be applied to Equation 7.

to a signal attenuation factor of  $\eta = 0.51$ .

For modeling the system noise temperature, the cryogenic electronics in Fig. 2 can be approximated as a cavity connected to the first-stage amplifier by a transmission line. The system noise temperature is then

$$T_n = T_{cav} + T_{amp} \quad (6)$$

where  $T_{cav}$  is the physical temperature of the cavity and  $T_{amp}$  is the noise temperature of the cryogenic amplifier. Boson statistics need not be considered in the Raleigh Jeans limit ( $k_b T_{cav} \gg hf$ ). The three isolators and the low-pass filter are not included in the thermal model because they are at the same temperature as the cavity. The electronics beyond the cryogenic amplifier are also not included in the thermal model because their contribution is suppressed by the Friis cascade equation [45]. The amplifier noise temperature  $T_{amp} = 4.9(5) \text{ K}$  dominates the system noise temperature. The cavity temperature, measured to be  $T_{cav} = 45(5) \text{ mK}$ , is much less than the uncertainty in  $T_{amp}$ .

The detector sensitivity is estimated from the operating parameters shown in Table I. The equation for sensitivity in  $\chi$  is

$$\chi = \sqrt{\frac{\beta + 1}{\beta} \frac{\text{SNR} \times b T_n}{m_{A'} \rho_{A'} V_{eff} Q_L}} \left( \frac{1}{b \Delta t} \right)^{1/4}. \quad (7)$$

Equation 7 is derived from rearranging the SNR equation. For this estimate, the bandwidth  $b$  is chosen to be comparable to cavity bandwidth. The SNR is also chosen to be two as this approximates a 90% exclusion limit. From the parameters in Table I, the sensitivity is estimated to be  $\chi = 2.4 \times 10^{-16}$ .

For the dark photon search, power from the cavity is measured using the Rohde & Schwarz FSW-26 Signal and Spectrum Analyzer. The cavity  $Q_L \sim 8 \times 10^9$ , so the frequency resolution needs to be  $b \sim 100 \text{ mHz}$ . This sub-Hertz resolution is achieved using the spectrum analyzer's I/Q-analyzer mode. For these measurements, a 312 Hz sample rate is used, and the sweep time of 10 s is used. The spectrum's center frequency is set to the cavity's

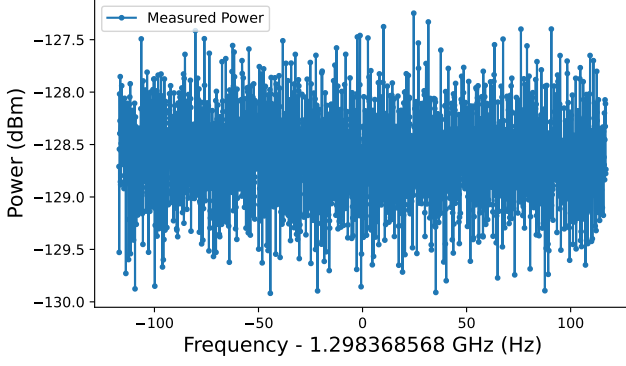


FIG. 5. Raw spectrum as measured by the spectrum analyzer. Assuming the spectrum is just noise, the raw spectrum is the noise power of the system.

resonant frequency. The frequency bin size is 100 mHz. The resulting power spectrum is shown in Fig. 5.

Once the power spectrum is measured, the standard haloscope analysis is applied to either find a spectrally narrow power excess consistent with a dark photon signal or to exclude parameter space. The procedure for deriving the exclusion limits follows the procedure developed by ADMX and HAYSTAC [43, 44, 46], and is adapted for dark photon searches [9, 10, 19].

There are a few important deviations from the standard haloscope analysis for this search. First, only one spectrum was measured, so there is no need to combine many spectra at different RF frequencies. Second, past haloscope experiments with  $Q_L \ll Q_{DM}$  typically convolved the spectra with the dark matter halo lineshape to account for the signal being spread across multiple bins. For this search,  $Q_L \gg Q_{DM}$ , so the signal will be Lorentzian from the cavity response. So the spectrum is convolved with the cavity lineshape  $L(f, f_0, Q_L) = 1/(1 + 4\Delta^2)$ . Third, a single measurement is sensitive to a range of dark photon masses. Thus the excluded power on resonance is convolved with the dark matter halo lineshape. This convolution was also performed in other dark photon searches with  $Q_L > Q_{DM}$  [47].

No spectrally narrow power excess with an  $\text{SNR} > 4$  is found in the measured power spectrum. The excluded parameter space using a 90% confidence limit is shown in Fig. 6. The derived limit assumes dark photon dark matter is randomly polarized and that the dark photon energy distribution follows the standard halo model. The excluded kinetic mixing strength is  $\chi_{90\%} = 2 \times 10^{-16}$  for a dark photon mass of  $m_{A'} = 5.370 \mu\text{eV}$ . This is consistent with the expected sensitivity estimated from Equation 7. This is also the deepest exclusion to wavelike dark photon dark matter by almost an order of magnitude.

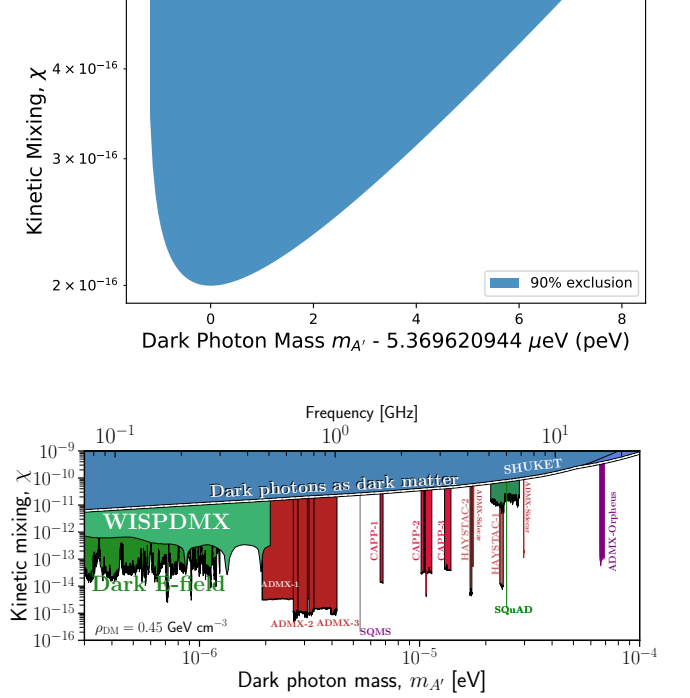


FIG. 6. Top: A 90% exclusion on the kinetic mixing strength parameter space. Bottom: SQMS limits in the context of other microwave cavity haloscopes. Figure adapted from [48].

### III. OUTLOOK AND THE POTENTIAL OF SRF CAVITIES FOR AXION DARK MATTER SEARCHES

The exclusion in Fig. 6 is an impressive demonstration of how SRF cavities can benefit dark matter searches. But an honest dark matter search with a finite probability of making a discovery requires that the haloscope tune through a wider range of frequencies. SQMS is currently developing experiments using tunable SRF cavities that will search through a wider range of parameter space.

In addition to dark photons, there is a growing interest in dark matter axions. Axions are particularly well motivated because they solve the strong CP problem [49]. Axion haloscope searches require multi-Tesla magnetic fields to be sensitive enough to the QCD axion. The scan rate for axion haloscope searches is still directly proportional to  $Q_L$ . Unfortunately, the performance of superconductors degrades under a multi-Tesla magnetic field. Achieving high quality factors is thus a very active area of research [35, 50–52], and it seems likely that axion haloscopes with  $Q_L > 10^6$  are achievable in the near future.

This experiment also demonstrates that axion haloscopes with  $Q_L \sim 10^{10}$  are worth striving for. Applying a hypothetical 8 T magnetic field to the dark photon data in Fig. 5 would have led to an exclusion on the axion-photon coupling constant at  $g_{a\gamma\gamma} \sim 4 \times 10^{-16}$ , well below DFSZ coupling ( $g_{a\gamma\gamma} = 8 \times 10^{-16}$ ).



Despite decades of searching for the axion, only a small fraction of the QCD axion parameter space has been explored. Perhaps a combination of ultra-high Q cavities, sub-SQL metrology [47, 53], multi-wavelength detector designs [24–31], and innovations in multi-Tesla continuous magnets will enable experiments to probe most of the post-inflation QCD axion parameter space within the next few decades.

#### IV. ACKNOWLEDGEMENTS

The authors thank Asher Berlin and Yonatan Kahn for fruitful discussions of scanning strategies with ultra-high

Q cavities. The authors thank Andrew Penhollow and Theodore C. Ill for the cavity assembling and locating the source of microphonics. This material is based upon work supported by the U.S. Department of Energy, Office of Science, National Quantum Information Science Research Centers, Superconducting Quantum Materials and Systems Center (SQMS) under contract number DE-AC02-07CH11359

- 
- [1] V. C. Rubin, W. K. Ford, Jr., N. Thonnard, and D. Burstein, Rotational properties of 23 SB galaxies, *Astrophys. J.* **261**, 439 (1982).
  - [2] K. G. Begeman, A. H. Broeils, and R. H. Sanders, Extended rotation curves of spiral galaxies: dark haloes and modified dynamics, *Monthly Notices of the Royal Astronomical Society* **249**, 523 (1991), <https://academic.oup.com/mnras/article-pdf/249/3/523/18160929/mnras249-0523.pdf>.
  - [3] A. N. Taylor, S. Dye, T. J. Broadhurst, N. Benitez, and E. van Kampen, Gravitational lens magnification and the mass of abell 1689, *The Astrophysical Journal* **501**, 539 (1998).
  - [4] P. Natarajan, U. Chadayammuri, M. Jauzac, J. Richard, J.-P. Kneib, H. Ebeling, F. Jiang, F. van den Bosch, M. Limousin, E. Jullo, H. Atek, A. Pillepich, C. Popa, F. Marinacci, L. Hernquist, M. Meneghetti, and M. Vogelsberger, Mapping substructure in the HST Frontier Fields cluster lenses and in cosmological simulations, *Monthly Notices of the Royal Astronomical Society* **468**, 1962 (2017), <https://academic.oup.com/mnras/article-pdf/468/2/1962/11210742/stw3385.pdf>.
  - [5] M. Markevitch, A. H. Gonzalez, D. Clowe, A. Vikhlinin, W. Forman, C. Jones, S. Murray, and W. Tucker, Direct constraints on the dark matter self-interaction cross section from the merging galaxy cluster 1e 0657-56, *The Astrophysical Journal* **606**, 819 (2004).
  - [6] N. Aghanim, Y. Akrami, M. Ashdown, J. Aumont, C. Baccigalupi, M. Ballardini, A. J. Banday, R. B. Barreiro, N. Bartolo, and et al., Planck 2018 results, *Astronomy & Astrophysics* **641**, A6 (2020).
  - [7] P. Zyla *et al.*, Review of Particle Physics, *PTEP* **2020**, 083C01 (2020).
  - [8] R. Essig, J. A. Jaros, W. Wester, P. H. Adrian, S. Andreas, T. Averett, O. Baker, B. Batell, M. Battaglieri, J. Beacham, T. Beranek, J. D. Bjorken, F. Bossi, J. R. Boyce, G. D. Cates, A. Celentano, A. S. Chou, R. Cowan, F. Curciarello, H. Davoudiasl, P. deNiverville, R. D. Vita, A. Denig, R. Dharmapalan, B. Dongwi, B. Döbrich, B. Echenard, D. Espriu, S. Fegan, P. Fisher, G. B. Franklin, A. Gasparian, Y. Gershtein, M. Graham, P. W. Graham, A. Haas, A. Hatzikoutelis, M. Holtrop, I. Irastorza, E. Izaguirre, J. Jaeckel, Y. Kahn, N. Kalantarians, M. Kohl, G. Krnjaic, V. Kubarovsky, H.-S. Lee, A. Lindner, A. Lobanov, W. J. Marciano, D. J. E. Marsh, T. Maruyama, D. McKeen, H. Merkel, K. Mofeit, P. Monaghan, G. Mueller, T. K. Nelson, G. R. Neil, M. Oriunno, Z. Pavlovic, S. K. Phillips, M. J. Pivovarovoff, R. Poltis, M. Pospelov, S. Rajendran, J. Redondo, A. Ringwald, A. Ritz, J. Ruz, K. Saenboonruang, P. Schuster, M. Shinn, T. R. Slatyer, J. H. Steffen, S. Stepanyan, D. B. Tanner, J. Thaler, M. E. Tobar, N. Toro, A. Upadye, R. V. de Water, B. Vlahovic, J. K. Vogel, D. Walker, A. Weltman, B. Wojtsekhowski, S. Zhang, and K. Zioutas, Dark sectors and new, light, weakly-coupled particles (2013), arXiv:1311.0029 [hep-ph].
  - [9] S. Ghosh, E. P. Ruddy, M. J. Jewell, A. F. Leder, and R. H. Maruyama, Searching for dark photons with existing haloscope data, *Phys. Rev. D* **104**, 092016 (2021).
  - [10] A. Caputo, A. J. Millar, C. A. J. O’Hare, and E. Vitagliano, Dark photon limits: A handbook, *Phys. Rev. D* **104**, 095029 (2021).
  - [11] B. Holdom, Searching for  $\epsilon$  charges and a new  $u(1)$ , *Physics Letters B* **178**, 65 (1986).
  - [12] B. Holdom, Two  $u(1)$ ’s and  $\epsilon$  charge shifts, *Physics Letters B* **166**, 196 (1986).
  - [13] M. Pospelov, A. Ritz, and M. Voloshin, Bosonic superwimps as kev-scale dark matter, *Phys. Rev. D* **78**, 115012 (2008).
  - [14] M. S. Turner, Periodic signatures for the detection of cosmic axions, *Phys. Rev. D* **42**, 3572 (1990).
  - [15] R. Jimenez, L. Verde, and S. P. Oh, Dark halo properties from rotation curves, *Monthly Notices of the Royal Astronomical Society* **339**, 243 (2003), <https://academic.oup.com/mnras/article-pdf/339/1/243/3557948/339-1-243.pdf>.
  - [16] P. W. Graham, J. Mardon, and S. Rajendran, Vector dark matter from inflationary fluctuations, *Phys. Rev. D* **93**, 103520 (2016).
  - [17] P. Arias, D. Cadamuro, M. Goodsell, J. Jaeckel, J. Redondo, and A. Ringwald, WISPy cold dark matter, *Journal of Cosmology and Astroparticle Physics* **2012** (06), 013.
  - [18] P. Sikivie, Experimental tests of the “invisible” axion, *Phys. Rev. Lett.* **51**, 1415 (1983).
  - [19] R. Cervantes, G. Carosi, C. Hanretty, S. Kimes, B. H. LaRoque, G. Leum, P. Mohapatra, N. S. Oblath, R. Ot-

- tens, Y. Park, G. Rybka, J. Sinnis, and J. Yang, Admx-orpheus first search for 70  $\mu\text{eV}$  dark photon dark matter: Detailed design, operations, and analysis (2022), arXiv:2204.09475.
- [20] D. Kim, J. Jeong, S. Youn, Y. Kim, and Y. K. Semertzidis, Revisiting the detection rate for axion haloscopes, *Journal of Cosmology and Astroparticle Physics* **2020** (03), 066.
- [21] P. Sikivie, Detection rates for “invisible”-axion searches, *Phys. Rev. D* **32**, 2988 (1985).
- [22] R. H. Dicke, The measurement of thermal radiation at microwave frequencies, *Review of Scientific Instruments* **17**, 268 (1946), <https://doi.org/10.1063/1.1770483>.
- [23] H. Peng *et al.*, Cryogenic cavity detector for a large scale cold dark-matter axion search, *Nucl. Instrum. Meth. A* **444**, 569 (2000).
- [24] R. Cervantes, G. Carosi, C. Hanretty, S. Kimes, B. H. LaRoque, G. Leum, P. Mohapatra, N. S. Oblath, R. Otens, Y. Park, G. Rybka, J. Sinnis, and J. Yang, Search for 70  $\mu\text{eV}$  dark photon dark matter with a dielectrically-loaded multi-wavelength microwave cavity (2022), arXiv:2204.03818.
- [25] P. Brun, A. Caldwell, L. Chevalier, G. Dvali, P. Freire, E. Garutti, S. Heyminck, J. Jochum, S. Knirck, M. Kramer, C. Krieger, T. Lasserre, C. Lee, X. Li, A. Lindner, B. Majorovits, S. Martens, M. Matysek, A. Millar, G. Raffelt, J. Redondo, O. Reimann, A. Ringwald, K. Saikawa, J. Schaffran, A. Schmidt, J. Schütte-Engel, F. Steffen, C. Strandhagen, G. Wieching, and M. A. D. M. A. X. Collaboration, A new experimental approach to probe qcd axion dark matter in the mass range above 40  $\mu\text{eV}$ , *The European Physical Journal C* **79**, 186 (2019).
- [26] A. Caldwell, G. Dvali, B. Majorovits, A. Millar, G. Raffelt, J. Redondo, O. Reimann, F. Simon, and F. Steffen (MADMAX Working Group), Dielectric haloscopes: A new way to detect axion dark matter, *Phys. Rev. Lett.* **118**, 091801 (2017).
- [27] M. Baryakhtar, J. Huang, and R. Lasenby, Axion and hidden photon dark matter detection with multilayer optical haloscopes, *Phys. Rev. D* **98**, 035006 (2018).
- [28] J. Chiles, I. Charaev, R. Lasenby, M. Baryakhtar, J. Huang, A. Roshko, G. Burton, M. Colangelo, K. V. Tilburg, A. Arvanitaki, S. W. Nam, and K. K. Berggren, First constraints on dark photon dark matter with superconducting nanowire detectors in an optical haloscope (2021), arXiv:2110.01582 [hep-ex].
- [29] B. T. McAllister, G. Flower, L. E. Tobar, and M. E. Tobar, Tunable supermode dielectric resonators for axion dark-matter haloscopes, *Phys. Rev. Applied* **9**, 014028 (2018).
- [30] A. P. Quiskamp, B. T. McAllister, G. Rybka, and M. E. Tobar, Dielectric-boosted sensitivity to cylindrical azimuthally varying transverse-magnetic resonant modes in an axion haloscope, *Phys. Rev. Applied* **14**, 044051 (2020).
- [31] M. Lawson, A. J. Millar, M. Pancaldi, E. Vitagliano, and F. Wilczek, Tunable axion plasma haloscopes, *Phys. Rev. Lett.* **123**, 141802 (2019).
- [32] C. Bartram, T. Braine, E. Burns, R. Cervantes, N. Crisosto, N. Du, H. Korandla, G. Leum, P. Mohapatra, T. Nitta, L. J. Rosenberg, G. Rybka, J. Yang, J. Clarke, I. Siddiqi, A. Agrawal, A. V. Dixit, M. H. Awida, A. S. Chou, M. Hollister, S. Knirck, A. Sonnenschein, W. Wester, J. R. Gleason, A. T. Hipp, S. Jois, P. Sikivie, N. S. Sullivan, D. B. Tanner, E. Lentz, R. Khatiwada, G. Carosi, N. Robertson, N. Woollett, L. D. Duffy, C. Boutan, M. Jones, B. H. LaRoque, N. S. Oblath, M. S. Taubman, E. J. Daw, M. G. Perry, J. H. Buckley, C. Gaikwad, J. Hoffman, K. W. Murch, M. Goryachev, B. T. McAllister, A. Quiskamp, C. Thomson, and M. E. Tobar (ADMX Collaboration), Search for invisible axion dark matter in the 3.3 – 4.2  $\mu\text{eV}$  mass range, *Phys. Rev. Lett.* **127**, 261803 (2021).
- [33] A. Romanenko, R. Pilipenko, S. Zorzetti, D. Frolov, M. Awida, S. Belomestnykh, S. Posen, and A. Grassellino, Three-dimensional superconducting resonators at  $t = 20$  mk with photon lifetimes up to  $\tau = 2$  s, *Phys. Rev. Applied* **13**, 034032 (2020).
- [34] B. Aune *et al.*, The superconducting TESLA cavities, *Phys. Rev. ST Accel. Beams* **3**, 092001 (2000), arXiv:physics/0003011.
- [35] S. Posen, M. Checchin, O. S. Melnychuk, T. Ring, and I. Gonin, Measurement of high quality factor superconducting cavities in tesla-scale magnetic fields for dark matter searches (2022).
- [36] A. Romanenko and D. I. Schuster, Understanding quality factor degradation in superconducting niobium cavities at low microwave field amplitudes, *Phys. Rev. Lett.* **119**, 264801 (2017).
- [37] S. Posen, A. Romanenko, A. Grassellino, O. Melnychuk, and D. Sergatskov, Ultralow surface resistance via vacuum heat treatment of superconducting radio-frequency cavities, *Phys. Rev. Applied* **13**, 014024 (2020).
- [38] *LNF-LNC0.3-14A 6-20 s/n 2122Z Cryogenic Low Noise Amplifier*, Low Noise Factory (2029).
- [39] J. Randa, E. Gerecht, D. Gu, and R. Billinger, Precision measurement method for cryogenic amplifier noise temperatures below 5 k, *IEEE Transactions on Microwave Theory and Techniques* **54**, 1180 (2006).
- [40] J. L. Cano, N. Wadefalk, and J. D. Gallego-Puyol, Ultra-wideband chip attenuator for precise noise measurements at cryogenic temperatures, *IEEE Transactions on Microwave Theory and Techniques* **58**, 2504 (2010).
- [41] H. Padamsee, J. Knobloch, and T. Hays, *RF Superconductivity for Accelerators, 2nd Edition* (Wiley-VCH, 2008).
- [42] O. Melnychuk, A. Grassellino, and A. Romanenko, Error analysis for intrinsic quality factor measurement in superconducting radio frequency resonators, *Review of Scientific Instruments* **85**, 124705 (2014), <https://doi.org/10.1063/1.4903868>.
- [43] B. M. Brubaker, L. Zhong, S. K. Lamoreaux, K. W. Lehnert, and K. A. van Bibber, Haystack axion search analysis procedure, *Phys. Rev. D* **96**, 123008 (2017).
- [44] C. Bartram, T. Braine, R. Cervantes, N. Crisosto, N. Du, G. Leum, L. J. Rosenberg, G. Rybka, J. Yang, D. Bowring, A. S. Chou, R. Khatiwada, A. Sonnenschein, W. Wester, G. Carosi, N. Woollett, L. D. Duffy, M. Goryachev, B. McAllister, M. E. Tobar, C. Boutan, M. Jones, B. H. LaRoque, N. S. Oblath, M. S. Taubman, J. Clarke, A. Dove, A. Eddins, S. R. O’Kelley, S. Nawaz, I. Siddiqi, N. Stevenson, A. Agrawal, A. V. Dixit, J. R. Gleason, S. Jois, P. Sikivie, J. A. Solomon, N. S. Sullivan, D. B. Tanner, E. Lentz, E. J. Daw, M. G. Perry, J. H. Buckley, P. M. Harrington, E. A. Henriksen, and K. W. Murch (ADMX Collaboration), Axion dark matter experiment: Run 1b analysis details, *Phys. Rev. D* **103**,

- 032002 (2021).
- [45] K. Blattenberger, Cascaded noise figure & noise temperature (2021).
  - [46] S. Asztalos, E. Daw, H. Peng, L. J. Rosenberg, C. Hagmann, D. Kinion, W. Stoeffl, K. van Bibber, P. Sikivie, N. S. Sullivan, D. B. Tanner, F. Nezrick, M. S. Turner, D. M. Moltz, J. Powell, M.-O. André, J. Clarke, M. Mück, and R. F. Bradley, Large-scale microwave cavity search for dark-matter axions, *Phys. Rev. D* **64**, 092003 (2001).
  - [47] A. V. Dixit, S. Chakram, K. He, A. Agrawal, R. K. Naik, D. I. Schuster, and A. Chou, Searching for dark matter with a superconducting qubit, *Phys. Rev. Lett.* **126**, 141302 (2021).
  - [48] C. O’Hare, cajohare/axionlimits: Axionlimits (2020).
  - [49] R. D. Peccei and H. R. Quinn, Cp conservation in the presence of pseudoparticles, *Phys. Rev. Lett.* **38**, 1440 (1977).
  - [50] D. Alesini, C. Braggio, G. Carugno, N. Crescini, D. D’Agostino, D. Di Gioacchino, R. Di Vora, P. Falferi, U. Gambardella, C. Gatti, G. Iannone, C. Ligi, A. Lombardi, G. Maccarrone, A. Ortolan, R. Pengo, C. Pira, A. Rettaroli, G. Ruoso, L. Taffarello, and S. Tocci, Realization of a high quality factor resonator with hollow dielectric cylinders for axion searches, *Nuclear Instruments and Methods in Physics Research Section A: Accelerators, Spectrometers, Detectors and Associated Equipment* **985**, 164641 (2021).
  - [51] R. Di Vora, D. Alesini, C. Braggio, G. Carugno, N. Crescini, D. D’Agostino, D. Di Gioacchino, P. Falferi, U. Gambardella, C. Gatti, G. Iannone, C. Ligi, A. Lombardi, G. Maccarrone, A. Ortolan, R. Pengo, A. Rettaroli, G. Ruoso, L. Taffarello, and S. Tocci, High- $q$  microwave dielectric resonator for axion dark-matter haloscopes, *Phys. Rev. Applied* **17**, 054013 (2022).
  - [52] D. Ahn, O. Kwon, W. Chung, W. Jang, D. Lee, J. Lee, S. W. Youn, H. Byun, D. Youm, and Y. K. Semertzidis, Biaxially textured  $\text{YBa}_2\text{Cu}_3\text{O}_{7-x}$  microwave cavity in a high magnetic field for a dark-matter axion search, *Phys. Rev. Applied* **17**, L061005 (2022).
  - [53] K. M. Backes, D. A. Palken, S. A. Kenany, B. M. Brubaker, S. B. Cahn, A. Droster, G. C. Hilton, S. Ghosh, H. Jackson, S. K. Lamoreaux, A. F. Leder, K. W. Lehnert, S. M. Lewis, M. Malnou, R. H. Maruyama, N. M. Rapidis, M. Simanovskaia, S. Singh, D. H. Speller, I. Urdinaran, L. R. Vale, E. C. van Asendelft, K. van Bibber, and H. Wang, A quantum enhanced search for dark matter axions, *Nature* **590**, 238 (2021).